Beamforming-Induced CSI Variations and Real-Time Security Feasibility in 6G THz V2X Networks

Vismaya KK
Department of Computer Science
Faculty of Science and Humanities
SRM Institute of Science and Technology
Kattankulathur, Tamil Nadu, India
vismayakootayi@gmail.com

Arul Leena Rose P.J
Department of Computer Applications
Faculty of Science and Humanities
SRM Institute of Science and Technology
Kattankulathur, Tamil Nadu, India
leena.rose527@gmail.com

D. Armstrong Doss
Department of Business Administration
Madras Christian College
Chennai, Tamil Nadu, India
armstrongdoss@gmail.com

***Abstract*—Terahertz (THz) vehicle-to-everything (V2X) links are a key 6G enabler due to abundant spectrum, but their highly directional beamforming reshapes physical-layer channel state information (CSI) in a manner that can be exploited for security-oriented situational awareness. This paper presents a compact, self-contained 300 GHz V2X simulation to quantify beamforming-induced CSI variations and to evaluate whether feature-based physical-layer analytics can meet strict 6G latency constraints. A balanced dataset of 1,000 samples is generated (500 legitimate, 500 alternative spatial observations) using a THz path-loss model with molecular absorption and a Gaussian beam pattern. Feature-importance analysis reveals that *beamforming gain* (0.3983) and *angle misalignment* (0.3211) dominate the CSI variation signature, followed by SNR (0.0919), RSS (0.0877), and path loss (0.0421). Computational measurements demonstrate microsecond-scale per-sample latency: 25.57 μs (Random Forest), 7.01 μs (SVM), and 1.09 μs (DNN), corresponding to throughputs of 39.1k, 142.8k, and 913.3k samples/s. The results demonstrate that beamforming-centric CSI signatures are both physically interpretable and computationally feasible for real-time security pipelines in 6G THz V2X systems.**

***Index Terms*—Beamforming, Channel State Information (CSI), Physical-layer security, Real-time feasibility, Latency analysis.**

I. Introduction

6G networks are expected to support ultra-reliable and low-latency communications for safety-critical applications such as cooperative perception and autonomous driving. One major direction is the use of THz spectrum above 100 GHz, where extremely large bandwidth becomes available [1]–[3]. However, THz propagation brings challenges such as high spreading loss and additional molecular absorption [4], motivating highly directional beamforming [5], [6].

In THz V2X, narrow beams improve link budget but also create strong spatial selectivity: small angular deviations can cause large gain and power variations. This introduces an opportunity to use beamforming-induced CSI variations as a *physical-layer signature* that may complement higher-layer security. Meanwhile, any practical 6G security analytics must respect strict timing constraints and should ideally consume only a small fraction of the 1 ms budget.

This paper is intentionally framed as a *feature-and-feasibility* study: rather than presenting a full intrusion detection protocol, we quantify (i) which CSI features dominate the spatial variation induced by THz beamforming, and (ii) whether real-time feature-based analytics is computationally feasible on typical compute platforms.

A. Contributions

- A reproducible 300 GHz V2X simulation including molecular absorption, narrow-beam Gaussian beamforming, mobility-induced Doppler, and small-scale fading.
- A CSI feature set (11 features) and a feature-importance analysis showing dominance of *beamforming gain* and *angle misalignment*.
- A computational performance study showing microsecond-scale per-sample latency for three representative inference models (RF/SVM/DNN), demonstrating real-time feasibility.

II. Related Work

THz communication is widely studied as a 6G candidate technology due to large contiguous spectrum and the emergence of highly directional links above 100 GHz [1], [2]. Channel modeling and wideband characterization for THz frequencies are summarized in surveys and measurement-driven studies [3]. Atmospheric absorption at THz is commonly modeled using established recommendations [4].

Beamforming is central to THz because it compensates for large path loss through high array gain [5]. Practical architectures (e.g., array-of-subarrays, hybrid beamforming) enable realizable THz beam management [6], [7]. In parallel, physical-layer security (PLS) has classical information-theoretic roots [8] and modern multi-antenna approaches that shape signals to improve confidentiality [9]. CSI has also been explored as a source of wireless signatures for authentication and spoofing/anomaly-related analysis at lower frequencies [10], [11].

For V2X, widely adopted security approaches emphasize PKI and upper-layer mechanisms [12], and realistic mobility/channel models are important for reproducible evaluation [13]. Finally, the feasibility of deploying machine learning inference at the edge has been studied in terms of efficiency and runtime characteristics [14], [15], motivating explicit latency evaluation for PHY analytics.

III. System and Channel Model

A. Scenario Parameters

We consider a highway-like V2X point-to-point link with:

- Carrier frequency $f_c = 300\,\text{GHz}$ (wavelength $\lambda = c/f_c \approx 1\,\text{mm}$),
- Beamwidth $\theta_{\text{BW}} = 5°$,
- Transmit power $P_{\text{TX}} = 30\,\text{dBm}$,
- Communication range up to 200 m,
- Vehicle speed around 30 m/s.

B. THz Path Loss with Molecular Absorption

We model total path loss as free-space path loss plus a distance-proportional absorption term:

$$\text{PL}(d) = 20\log_{10}(d) + 20\log_{10}(f_c) + 20\log_{10}\left(\frac{4\pi}{c}\right) + \alpha d, \tag{1}$$

where d is distance (m), c is the speed of light, and α is the absorption coefficient (dB/m). We use $\alpha = 0.1\,\text{dB/m}$ consistent with short-range THz operation.

C. Directional Beamforming Gain

Beamforming gain depends on the angular mismatch between beam pointing and target direction. We use a Gaussian beam pattern:

$$G_{\text{BF}}(\Delta\theta) = G_{\max}\exp\left(-\frac{\Delta\theta^2}{2\theta_{\text{BW}}^2}\right), \tag{2}$$

where $G_{\max} = 30\,\text{dB}$ and $\Delta\theta$ is the absolute angle misalignment in degrees.

D. Received Power, SNR, and Doppler

Received power (dBm) is:

$$P_{\text{RX}} = P_{\text{TX}} + G_{\text{BF}} - \text{PL}(d). \tag{3}$$

SNR is computed relative to noise floor $N_0 = -90\,\text{dBm}$:

$$\text{SNR} = P_{\text{RX}} - N_0. \tag{4}$$

Doppler shift is modeled as:

$$f_D = \frac{v}{c} f_c \cos(\Delta\theta), \tag{5}$$

where v is the TX speed.

IV. CSI Feature Set and Dataset

A. Feature Set

We extract 11 features per sample:

- distance, rss, path_loss, beamforming_gain, angle_misalignment, doppler_shift,
- delay_spread (ns), phase, channel_gain, snr, rayleigh_fading.

TABLE I
Simulation parameters used in the 300 GHz THz V2X study.

Parameter	Value
Carrier frequency (f_c)	300 GHz
Wavelength (λ)	1.00 mm
Beamwidth (θ_{BW})	5°
Transmit power (P_{TX})	30 dBm
Noise floor (N_0)	-90 dBm
Molecular absorption (α)	0.1 dB/m
Communication range	up to 200 m
Vehicle speed	25–35 m/s (typical)
Dataset size	1000 samples (500/500)
Number of features	11

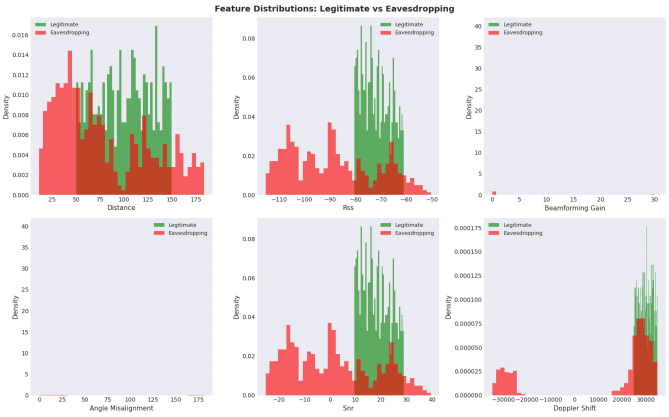

Fig. 1. Feature distributions illustrating beamforming-induced CSI variation (legitimate vs. alternative spatial observations).

B. Dataset Generation

A balanced dataset of 1000 samples is generated:

- **Legitimate** (500): RX placed 50–150 m ahead of TX with lateral offset ±5 m; beam points toward RX.
- **Alternative observations** (500): observation points distributed across four spatial strategies (side/behind/between/far) while the beam still points toward RX.

V. Results: Feature-Driven CSI Variation

This section reports empirical evidence that beamforming-centric features dominate CSI variation under THz directionality.

A. Feature Distributions

Fig. 1 shows the distributions of representative features. Clear separation is visible for beamforming gain, angle misalignment, RSS, and SNR, whereas Doppler exhibits broader overlap due to geometry and velocity projection.

B. Correlation Structure

Fig. 2 presents the correlation matrix among the extracted features. Notably, RSS and SNR correlate strongly with beamforming gain due to their dependence on link budget, while distance correlates strongly with path loss.

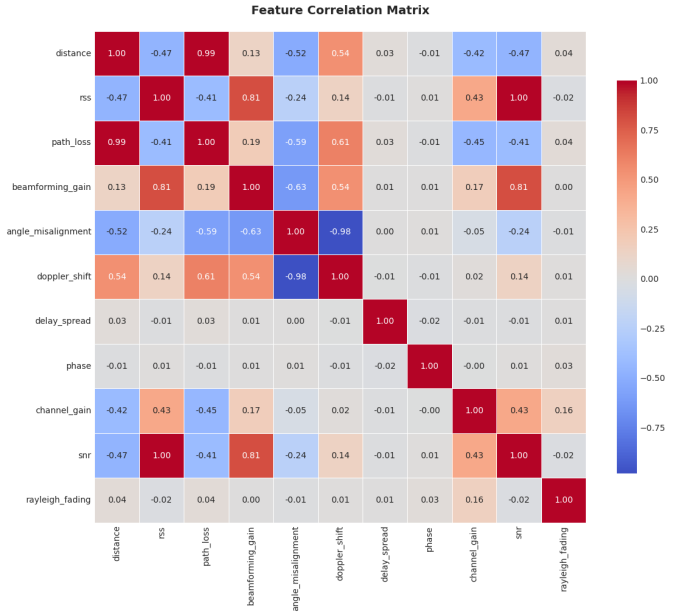

Fig. 2. Correlation matrix of CSI features in the simulated 300 GHz V2X dataset.

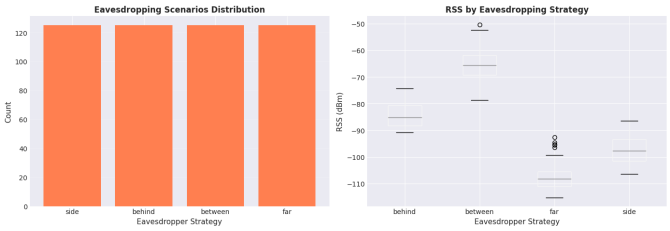

Fig. 3. Alternative observation strategy distribution and RSS by strategy.

C. Scenario Composition

Fig. 3 summarizes alternative observation strategies and RSS variability by strategy. Even when an observation point lies closer to the beam path ("between"), the beam alignment and gain properties still induce distinct link-budget behavior relative to legitimate alignment.

D. Feature Importance

We quantify which features explain the largest share of the observed variation using a Random Forest feature-importance analysis. The top five features are:

- beamforming_gain: 0.3983
- angle_misalignment: 0.3211
- snr: 0.0919
- rss: 0.0877
- path_loss: 0.0421

Beamforming-centric features dominate:

$$0.3983 + 0.3211 = 0.7194 \approx 71.94\%, \tag{6}$$

indicating that nearly 72% of the variation signature is explained by beam alignment and the resulting beamforming gain.

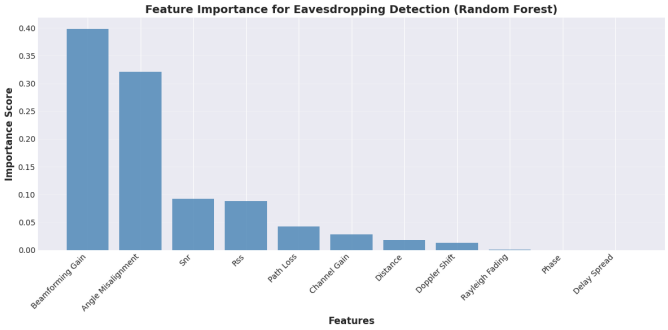

Fig. 4. Feature importance (Random Forest): beamforming gain and angle misalignment dominate the CSI variation signature.

TABLE II
TOP-5 MOST IMPORTANT CSI FEATURES (RANDOM FOREST IMPORTANCE).

Rank	Feature	Importance
1	beamforming_gain	0.3983
2	angle_misalignment	0.3211
3	snr	0.0919
4	rss	0.0877
5	path_loss	0.0421

VI. Computational Feasibility

To evaluate real-time feasibility under a 6G budget, we measure average inference time, per-sample latency, and throughput for three representative models (RF/SVM/DNN).

All approaches satisfy the 6G < 1 ms constraint with large margin:

$$25.57\,\mu s,\ 7.01\,\mu s,\ 1.09\,\mu s \ll 1000\,\mu s. \tag{7}$$

VII. Discussion

A. Key Takeaways

(1) Beamforming dominates CSI variation. The feature-importance ranking indicates that beamforming gain and angle misalignment jointly explain 71.94% of the variation signature, consistent with pencil-beam behavior at 300 GHz.

(2) Secondary features inherit beam effects. RSS and SNR appear as secondary features because they are direct functions of beamforming gain and path loss.

(3) Real-time feasibility is strong. The measured microsecond-scale latency implies that such feature-based analytics can run comfortably within 6G timing constraints, leaving headroom for PHY/MAC processing.

B. Limitations

This work is simulation-based and uses a simplified Gaussian beam pattern and constant absorption coefficient. Future work should incorporate measurement-informed THz models, explicit beam-tracking error dynamics, blockage, and multi-vehicle interactions.

TABLE III
COMPUTATIONAL PERFORMANCE OF PER-SAMPLE CSI ANALYTICS (CPU).

Model	Avg. time (ms)	Latency/sample (μs)	Throughput
Random Forest	7.67	25.57	39,106
SVM	2.10	7.01	142,752
DNN	0.33	1.09	913,255

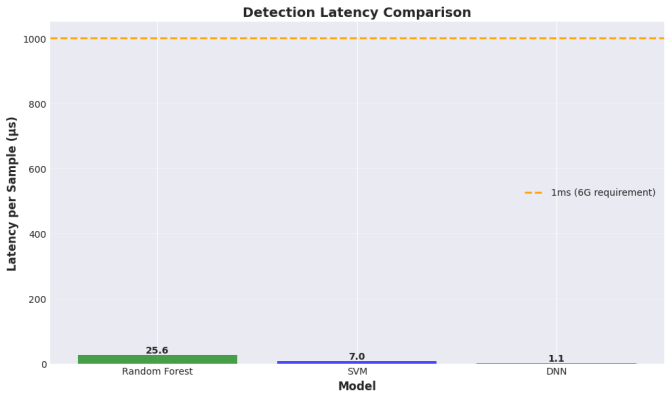

Fig. 5. Per-sample analysis latency for RF/SVM/DNN compared against the 1 ms (6G) budget.

VIII. CONCLUSION

This paper presented a feature-and-feasibility study of beamforming-induced CSI variations in 6G THz V2X networks at 300 GHz. Feature-importance analysis shows that beamforming gain (0.3983) and angle misalignment (0.3211) dominate the variation signature (71.94% combined). Computational results show per-sample inference latency of 25.57 μs (RF), 7.01 μs (SVM), and 1.09 μs (DNN), far below the 1 ms 6G constraint. These findings support the feasibility of lightweight, interpretable physical-layer analytics driven by beamforming-centric CSI features in future THz V2X systems.

REFERENCES

[1] T. S. Rappaport, Y. Xing, O. Kanhere, S. Ju, A. Madanayake, S. Mandal, A. Alkhateeb, and G. Trichopoulos, "Wireless communications and applications above 100 GHz: Opportunities and challenges for 6G and beyond," IEEE Access, vol. 7, pp. 78729–78757, 2019, doi: 10.1109/ACCESS.2019.2921522.

[2] I. F. Akyildiz, C. Han, and S. Nie, "Combating the distance problem in the millimeter wave and terahertz frequency bands," IEEE Commun. Mag., vol. 56, no. 6, pp. 102–108, Jun. 2018, doi: 10.1109/MCOM.2018.1700928.

[3] C. Han, A. Bicen, and I. F. Akyildiz, "Multi-ray channel modeling and wideband characterization for wireless communications in the terahertz band," IEEE Trans. Wireless Commun., vol. 14, no. 5, pp. 2402–2412, May 2015, doi: 10.1109/TWC.2014.2386335.

[4] ITU-R (2019) Attenuation by Atmospheric Gases and Related Effects. Recommendation P.676-12, Electronic Publication, Geneva.

[5] C. Lin and G. Y. Li, "Terahertz communications: An array-of-subarrays solution," IEEE Commun. Mag., vol. 54, no. 12, pp. 124–131, Dec. 2016, doi: 10.1109/MCOM.2016.1600306CM.

[6] C. Han, L. Yan, and J. Yuan, "Hybrid beamforming for terahertz wireless communications: Challenges, architectures, and open problems," arXiv preprint arXiv:2101.08469, Jan. 2021, doi: 10.48550/arXiv.2101.08469.

[7] M. Giordani, M. Polese, A. Roy, D. Castor, and M. Zorzi, "A tutorial on beam management for 3GPP NR at mmWave frequencies," IEEE Commun. Surveys Tuts., vol. 21, no. 1, pp. 173–196, First Quart. 2019, doi: 10.1109/COMST.2018.2869411.

[8] A. D. Wyner, "The Wiretap Channel," Bell System Technical Journal, Vol. 54, No. 8, 1975, pp. 1355-1367. doi:10.1002/j.1538-7305.1975.tb02040.x

[9] S. Goel and R. Negi, "Guaranteeing secrecy using artificial noise," IEEE Trans. Wireless Commun., vol. 7, no. 6, pp. 2180–2189, Jun. 2008, doi: 10.1109/TWC.2008.060848.

[10] Y. Chen, W. Trappe, and R. P. Martin, "Detecting and localizing wireless spoofing attacks," in Proc. IEEE 4th Annu. Commun. Soc. Conf. Sensor, Mesh Ad Hoc Commun. Netw. (SECON), Jun. 2007, pp. 193–202, doi: 10.1109/SAHCN.2007.4292831.

[11] L. Xiao, L. J. Greenstein, N. B. Mandayam, and W. Trappe, "Using the physical layer for wireless authentication in time-variant channels," IEEE Trans. Wireless Commun., vol. 7, no. 7, pp. 2571–2579, Jul. 2008, doi: 10.1109/TWC.2008.070194.

[12] ETSI TS 102 940, "Intelligent Transport Systems (ITS); Security; ITS communications security architecture and security management," European Telecommunications Standards Institute, 2021.

[13] M. Boban, J. Barros, and O. K. Tonguz, "Geometry-based vehicle-to-vehicle channel modeling for large-scale simulation," IEEE Trans. Veh. Technol., vol. 63, no. 9, pp. 4146–4164, Nov. 2014, doi: 10.1109/TVT.2014.2317803.

[14] V. Sze, Y.-H. Chen, T.-J. Yang, and J. S. Emer, "Efficient processing of deep neural networks: A tutorial and survey," arXiv preprint arXiv:1703.09039, Mar. 2017, doi: 10.48550/arXiv.1703.09039.

[15] M. A. Nielsen, *Neural Networks and Deep Learning*. Determination Press, 2015. [Online]. Available: http://neuralnetworksanddeeplearning.com/